The Sea Surface Temperature Pattern Effect on Outgoing Longwave Radiation: the Role of Large-scale Convective Aggregation

Heng Quan [1,2], Bosong Zhang [2], Chenggong Wang [1,2], Stephan Fueglistaler [1,2]

[1]Department of Geosciences, Princeton University, Princeton, NJ, US
[2]Program in Atmospheric and Oceanic Sciences, Princeton University, Princeton, NJ, US

Key Points:

- Tropical SST gradients affect OLR by modulating the strength of large-scale convective aggregation
- The SST pattern effect on OLR is comparable to that on shortwave cloud radiative effect, both with large inter-model spread
- The large-scale convective aggregation post 1980 contributes to a more stabilizing climate feedback than that expected for future

Corresponding author: Heng Quan, `hengquan@princeton.edu`

Abstract

Observations and climate models show a strong increase/decrease of tropical low clouds, and hence reflected solar radiation, to an increase/decrease of the west-east sea surface temperature gradient in the tropical Pacific due to its impact on boundary layer inversion strength. Here, we show that the cloud shortwave radiative effect is amplified by the longwave radiation response due to a mean drying/moistening of the tropical free troposphere, and a decrease/increase of high cloud amount, resulting from the contraction/expansion of the area of tropical deep convection. This large-scale convective aggregation mechanism substantially amplifies the negative shortwave cloud feedback due to the post 1980 La-Nina-like SST warming pattern. The connection between the shortwave cloud radiative effect and longwave radiative effect is physically plausible and robust among models, but their relative magnitude shows large inter-model spread pointing to an underappreciated climate model uncertainty.

Plain Language Summary

The top-of-atmosphere radiation is not only determined by the global mean surface temperature, but is also affected by its spatial pattern, especially the pattern of tropical Sea Surface Temperature (SST). Previous studies found that a larger west-east SST gradient in the tropical Pacific increases the low cloud amount, resulting in more reflection of incoming solar radiation. Here, we demonstrate that a larger tropical SST gradient also increases the outgoing longwave radiation emitted by the Earth. This is because a larger SST gradient narrows the area of tropical deep convection with abundant water vapor and high clouds, and expands the non-convective area which is much drier and has fewer high clouds. Consequently, the atmosphere (on average) becomes more transparent to longwave radiation, resulting in more longwave emission to space. Thus, for an SST trend pattern as observed post 1980, the pattern results in a negative feedback for both the cloud shortwave feedback and the longwave feedback compared to a uniform warming case. When averaged over different climate models, the cloud shortwave and longwave feedback response to patterned warming are of similar magnitude, but individual models may have substantially different feedback ratios, pointing to an underappreciated climate model uncertainty.

1 Introduction

The responses of the climate system to global warming are commonly normalized by the change in global mean surface temperature. The climate feedback ($\lambda, [\mathrm{Wm}^{-2}\mathrm{K}^{-1}]$) (the inverse of which sets the "climate sensitivity") is defined as the change of the top of atmosphere (TOA) net radiation per Kelvin global mean surface warming. However, recent studies have shown that in particular the geographical sea surface temperature (SST) warming pattern in the tropical Pacific over the historical period may strongly modulate the TOA net radiation response (Stevens et al., 2016; Gregory & Andrews, 2016; Zhou et al., 2017; Dong et al., 2019; Fueglistaler, 2019; Fueglistaler & Silvers, 2021; Ceppi & Fueglistaler, 2021; Williams et al., 2023).

Generally, the focus of these analyses has been the impact of patterned SST trends on the average shortwave cloud radiative effect, which we summarize in Fig. 1: Due to the weak temperature gradient in free-troposphere close to equator (Charney, 1963; Sobel et al., 2001) and the fact that deep convection at high SSTs (i.e. the western Pacific warm pool) couples the free-tropospheric temperature to the surface temperature in these regions (Arakawa & Schubert, 1974; Emanuel et al., 1994), variations in the west-east SST gradient in the tropical Pacific directly lead to variations in the average boundary layer inversion strength. The latter, in turn, strongly affects in particular low cloud occurrence (Klein & Hartmann, 1993; Wood & Bretherton, 2006) and hence the global shortwave cloud radiative effect.

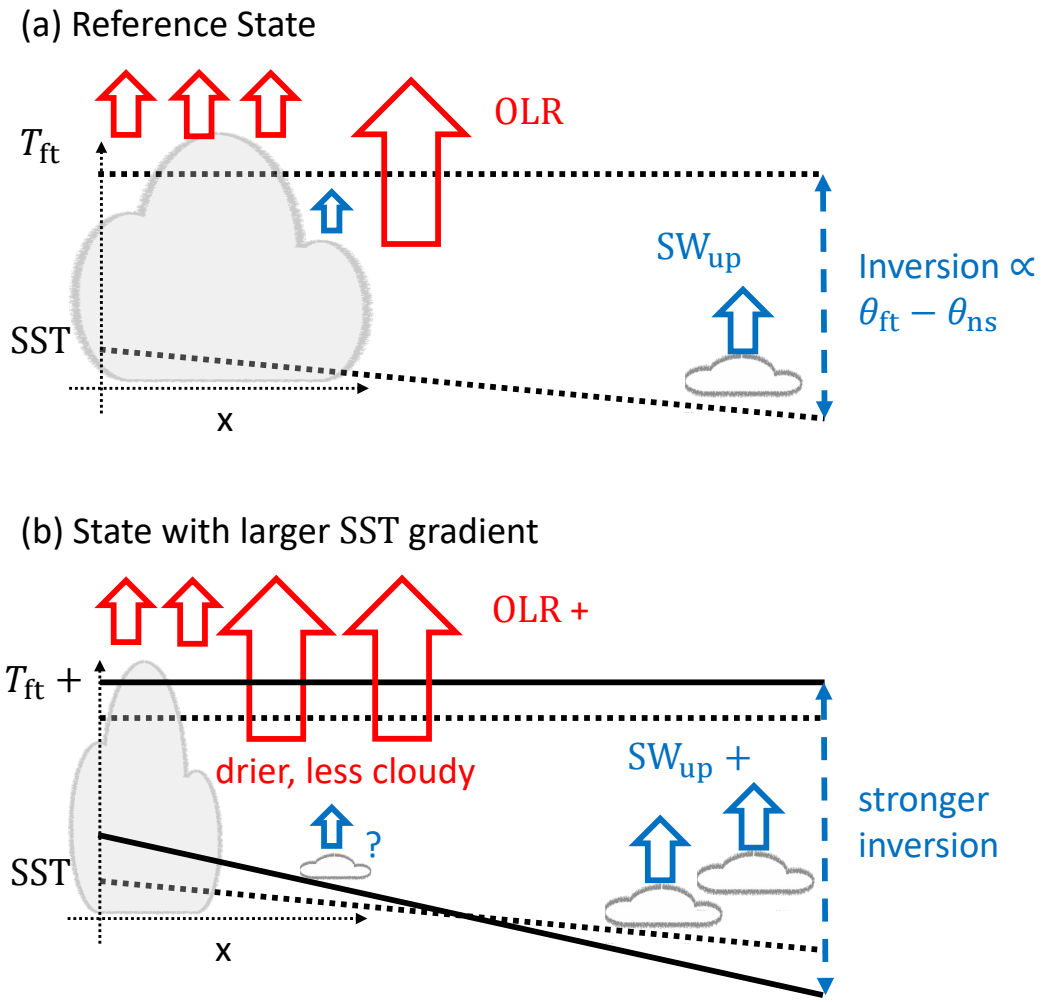

Figure 1. Schematic of the impact of the SST gradient on cloud shortwave radiative effect, and outgoing longwave radiation. The temperature of the free troposphere (T_{ft}) is set by the SST at the warm end of the domain where deep convection couples the boundary layer to the free troposphere. A steepening of the SST gradient (lower panel) relative to a reference state (upper panel), results in an increase in the boundary layer inversion strength (approximately proportional to the difference between free-tropospheric potential temperature and near-surface potential temperature, $\theta_{\mathrm{ft}} - \theta_{\mathrm{ns}}$) over the cold part of the domain, leading to more low clouds and more reflected shortwave radiation (blue arrows). A larger SST gradient also results in the large-scale aggregation of tropical deep convection due a higher (relative to the mean) convective threshold (Neelin et al., 2003; Chou & Neelin, 2004; Y. Zhang & Fueglistaler, 2019) and stronger up-gradient boundary layer moisture transport (Quan et al., 2024). This large-scale convective aggregation reduces the free-tropospheric relative humidity and high cloud amount, resulting in an increase in outgoing longwave radiation (OLR, red arrows) (Bony et al., 2020; Becker & Wing, 2020; B. Zhang et al., 2021; Schiro et al., 2022; McKim et al., 2021; Feng et al., 2023). Note that the shortwave cloud radiative effect change in the region of deep convection is less unambiguous (and not discussed in this paper) since low clouds could compensate for the reduction of high clouds (indicated with question mark).

In the following, we argue that the magnitude of the impact of the tropical SST gradient on outgoing longwave radiation (OLR) through its control on the large-scale aggregation of deep convection (Fig. 1) is comparable to its impact on the shortwave cloud radiative effect.

The paper is organized as follows. Section 2 describes the numerical models and simulations used in this study. Section 3 presents the main results: (i) Idealized SST gradient perturbation simulations demonstrate that the tropical SST gradient affects OLR primarily by modulating the strength of large-scale convective aggregation; and (ii) targeted atmospheric GCM simulations with prescribed sea surface temperatures and fixed pre-industrial forcings (similar to the CMIP6 amip piControl experiment) show that the post 1980 large-scale convective aggregation due to the La-Nina-like SST warming pattern is the main cause of the enhanced OLR increase relative to a uniform SST warming pattern. This longwave effect is comparable to and amplifies the enhanced shortwave cloud radiative effect, and contributes to a more negative (stabilizing) climate feedback post 1980 than that expected based on coupled atmosphere-ocean GCMs for long-term CO_2 increase. Finally, Section 4 summarizes the results and conclusions, and discusses implications.

2 Methods

2.1 General Circulation Model (GCM) simulations

We use the Geophysical Fluid Dynamics Laboratory (GFDL) atmospheric general circulation model AM4 (Zhao et al., 2018a, 2018b) to conduct SST perturbation simulations. AM4 uses a horizontal grid spacing of approximately 100 km and saves the data to disk on a grid with 180 grid points in the meridional, and 288 grid point in the zonal direction (i.e. $1.0^\circ \times 1.25^\circ$ for the horizontal resolution). The SST perturbations (defined below) are applied to a control simulation forced by the observed climatological (1982-2001) monthly means of SSTs and sea ice concentrations from the HADISST1 dataset (Rayner et al., 2003). The greenhouse gas concentrations and aerosol emissions correspond to the conditions of the year 2000 and are not modified in the perturbation simulations. The control simulation and the perturbation simulations are integrated for 45 years, with the first 5 years discarded to eliminate spin-up effects. All results below show averaged fields computed from the monthly mean fields of the last 40 years of the model simulations.

The following perturbations are applied to the control state SSTs:

1. Idealized tropical SST gradient perturbation simulations. Following Fueglistaler (2019), we quantify the tropical (between 30°S to 30°N) SST gradient by $\mathrm{SST}^{\#}$, defined as the average temperature of the warmest 30% minus the tropical average SST. For any target $\mathrm{SST}^{\#}_{\mathrm{target}}$, the tropical SST field (between 30°S to 30°N) in the perturbation simulation is given by

$$\mathrm{SST} = \overline{\mathrm{SST}}_{\mathrm{control}} + \frac{\mathrm{SST}^{\#}_{\mathrm{target}}}{\mathrm{SST}^{\#}_{\mathrm{control}}} \times \left(\mathrm{SST}_{\mathrm{control}} - \overline{\mathrm{SST}}_{\mathrm{control}}\right), \qquad (1)$$

   where "control" denotes the control simulation and the overbar symbol stands for the average over the tropics. SSTs outside the tropics are not perturbed. The SST perturbation as specified in equation 1 perturbs the tropical SST gradient without changing the tropical average SST. The control simulation has $\mathrm{SST}^{\#} = 2.45\,\mathrm{K}$, and we run ten perturbation simulations covering the range from $\mathrm{SST}^{\#} = 0.5\,\mathrm{K}$ to $\mathrm{SST}^{\#} = 5.0\,\mathrm{K}$ (with an increment of $0.5\,\mathrm{K}$).
2. A simulation using the SST trend pattern of the period 1980 to 2010, where the local SST perturbation equals to the linear trend (at each grid cell) of the HADISST1

SST data (Rayner et al., 2003) from 1980 to 2010; the experiment applies the effective change over the 30 years as given by the linear regression.
3. A uniform SST +4 K simulation for comparison with the patterned warming simulation.

2.2 Cloud-Resolving Model (CRM) simulations

We use the version 6.11.5 of the System for Atmospheric Modeling (SAM) cloud resolving model (CRM) (Khairoutdinov & Randall, 2003), which is an anelastic nonhydrostatic model with bulk microphysics. The model uses a simple Smagorinsky-type scheme to represent the effect of subgrid-scale turbulence, and computes the surface sensible heat, latent heat and momentum fluxes by the Monin–Obukhov similarity theory.

We perform 2-D (x-z) mock Walker (similar to Kuang (2012) and Wofsy and Kuang (2012)) simulations without rotation. The vertical grid has 64 levels, starting at 25 m and extending up to 27 km, and the vertical grid spacing increases from 50 m at the lowest levels to roughly 1 km at the top of the domain. The model has a rigid lid at the top with a wave-absorbing layer occupying the upper third of the domain to prevent the reflection of gravity waves. The domain width along the x-direction is $L = 10240$ km with a 2-km horizontal resolution, and solid wall boundary conditions are employed on both sides.

We use the CAM interactive radiation scheme and a fixed incoming solar radiation of $650.83 \mathrm{W m^{-2}}$ with a zenith angle of 50.5° (Lutsko, 2018). The prescribed SSTs have a mean value of 300 K and linearly decrease by ΔSST from the left boundary ($x = 0$) to the right boundary ($x = 10240$ km). Six simulations covering the range of $\Delta\mathrm{SST} =$ 5 K to 10 K (with an increment of 1 K) are run for 150 days and reach steady state after approximately 50 days. All results shown from these simulations are averaged fields computed from the last 50 days of hourly model output.

3 Results

3.1 The role of large-scale convective aggregation

We first show the results of the idealized SST gradient perturbation simulations (Section 2). Figure 2(a,d) shows that both OLR and reflected (upward) shortwave radiation ($\mathrm{SW_{up}}$) increase with increasing tropical SST gradient (measured by $\mathrm{SST}^{\#}$) in the AM4 simulations, and they have a similar sensitivity to the SST gradient perturbation. The response of $\mathrm{SW_{up}}$ quantitatively supports the qualitative expectation that an increase (decrease) of the tropical SST gradient warms (cools) the tropical free-troposphere, resulting in a stronger (weaker) boundary layer inversion (Fig. 2(b)) and more (less) low clouds (Fig. 2(c)) especially above cold SSTs that reflect more (less) solar radiation.

The increase in OLR with increasing $\mathrm{SST}^{\#}$ but fixed average SST (Fig. 2(d)) is the focus of this paper. At fixed relative humidity, the clear-sky OLR is approximately linearly related to the (average) surface temperature (Y. Zhang et al., 2020; McKim et al., 2021), which cannot explain the approximately linear relation between OLR and $\mathrm{SST}^{\#}$ in the model simulation. Thus, Fig. 2(d) highlights the impact of large-scale convective aggregation on OLR. As the SST gradient becomes larger, the resultant warming of the tropical free-troposphere raises the threshold (relative to the mean SST) of deep convection. The free-tropospheric moist static energy (MSE) increase is approximately spatially uniform due to the WTG approximation (Charney, 1963; Sobel et al., 2001) and set by the near-surface MSE increase above the warmest SSTs through deep convection (Arakawa & Schubert, 1974; Emanuel et al., 1994; Y. Zhang & Fueglistaler, 2020), and regions whose subcloud MSE increases less than that in the region of the warm SSTs are no longer convective (Neelin et al., 2003; Y. Zhang & Fueglistaler, 2019). A larger SST gradient also

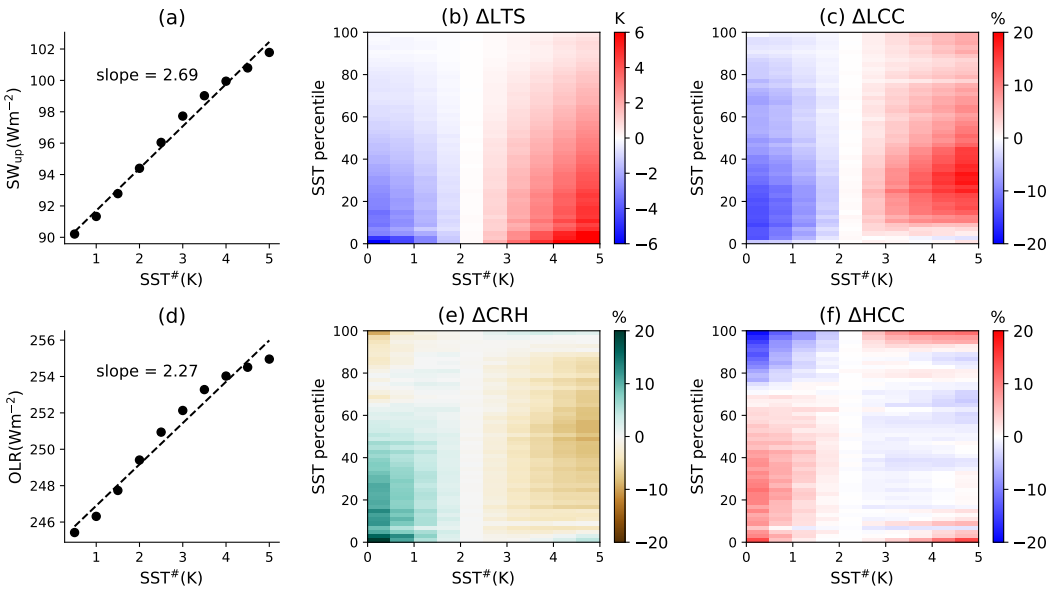

Figure 2. Tropical (30°S to 30°N) average (a) TOA upward shortwave radiation (SW_{up}) and (d) OLR for AM4 simulations with different SST$^{\#}$. (b)(c)(e)(f) Responses (perturbation run minus control run) of tropical (30°S to 30°N) mean static stability of lower troposphere (LTS, the difference between 700 hPa potential temperature and sea level potential temperature), low cloud cover (LCC), column relative humidity (CRH, water vapor mass divided by saturated water vapor mass between 850 hPa and 200 hPa) and high cloud cover (HCC) for AM4 simulations with different SST$^{\#}$, binned into SST percentiles, with sorting from cold (percentile 1) to warm (percentile 100).

causes a stronger boundary layer circulation (Lindzen & Nigam, 1987), which increases the up-gradient moisture transport from subsiding regions to convective regions (Quan et al., 2024).

These two effects together cause a stronger large-scale convective aggregation (i.e. a narrowing of the convective area) associated with the expansion of dry and clear-sky regions. As shown by Fig. 2(e) and (f), a larger (smaller) SST gradient causes the decrease (increase) of column relative humidity (CRH) and high cloud amount at the intermediate SST percentiles, which increases (decreases) the tropical average OLR. This response is consistent with the relation between convective organization and OLR reported in previous studies (Bony et al., 2020; Becker & Wing, 2020; Schiro et al., 2022) and confirms the schematic in Fig. 1. Note, however, that the aggregation of interest here occurs on the planetary scale, rather than in small-domain cloud resolving simulations without external forcing (e.g. Muller and Held (2012); Wing et al. (2018)).

The large-scale convective aggregation seen in the GCM simulations (Fig. 2) may be unduly affected by parameterizations in particular of the convective processes. The CRM mock-Walker simulations (Section 2) rely on fewer parameterizations and explicity resolve deep convection. We find that the CRM mock-Walker simulations show (Supplement Fig. S1 and S2) the same effect as the GCM simulations, adding confidence that the GCM results are physically robust and not unduly affected by parameterizations and uncertainties therein.

Because global warming experiments with coupled atmosphere-ocean GCMs yield only a small amplification (order 10%) of the tropical SST gradient (Fueglistaler & Silvers, 2021), neither the shortwave nor the longwave radiation responses in these simulations show a strong signature of departure from the responses to uniform SST warming (Schiro et al., 2022). However, the situation is very different for the observations over the historical period. In particular, between the late 1970s and early 2000s, the amplification of the tropical SST gradient is about 50% (Fueglistaler & Silvers, 2021), which induces a strong negative feedback (Fueglistaler & Silvers, 2021; Armour et al., 2024).

3.2 The effect of post 1980 SST trend patterns on OLR

In the following, we quantify the contribution of large-scale convective aggregation to the negative longwave feedback in the historical period. We compare the radiative flux responses (normalized by tropical average surface temperature change) of the AM4 atmospheric GCM with prescribed uniform +4 K SST increase to the simulation with the patterned historical SST change over the period 1980-2010 (see Section 2). Table 1 summarizes what we define as the "historical pattern effect": the difference "historical patterned warming" simulation minus "uniform warming" simulation.

The results in Table 1 are consistent with the expectations as shown in the schematic (Fig. 1): Compared with the uniform +4 K simulation, the response of the historical simulation with a La-Nina-like SST warming pattern shows a larger increase in reflected shortwave radiation of $\Delta\frac{\mathrm{dSW_{up}}}{\mathrm{d}\overline{T_s}} = 1.93\mathrm{Wm^{-2}K^{-1}}$ and a larger increase of OLR of $\Delta\frac{\mathrm{dOLR}}{\mathrm{d}\overline{T_s}} = 1.45\mathrm{Wm^{-2}K^{-1}}$. The table further shows the change in lower tropospheric stability (LTS), low cloud cover (LCC), column relative humidity (CRH), and high cloud cover (HCC); and their differences between the two experiments. The table shows that the larger $\mathrm{SW_{up}}$ increase is due to an enhanced increase in lower troposphere stability and low cloud amount, while the larger OLR increase is due to enhanced free-tropospheric warming, free-tropospheric drying and high cloud reduction. Note that the sign of the changes provides support to the physical reasoning (Fig. 1), and the numerical simulations reveal that the magnitude of the shortwave and longwave effect are very similar for this atmospheric GCM. While the sign of the OLR trend difference is as expected considering the large-scale aggregation mechanism, further analysis is needed to provide proof that the cause is indeed large scale aggregation and not other processes (e.g. free-tropospheric warming only).

Table 1. Tropical (30°S to 30°N) average responses of six variables (identical to variables in Fig. 2) normalized to +1 K tropical mean surface warming for the AM4 historical (post 1980) SST perturbation simulation, AM4 uniform SST +4 K simulation and their difference (historical minus uniform +4 K).

	Historical	Uniform +4 K	Difference
$\frac{\mathrm{dSW_{up}}}{\mathrm{d}\overline{T_s}}(\mathrm{Wm^{-2}K^{-1}})$	1.72	-0.21	1.93
$\frac{\mathrm{dOLR}}{\mathrm{d}\overline{T_s}}(\mathrm{Wm^{-2}K^{-1}})$	3.14	1.69	1.45
$\frac{\mathrm{dLTS}}{\mathrm{d}\overline{T_s}}(\mathrm{KK^{-1}})$	0.66	0.32	0.34
$\frac{\mathrm{dLCC}}{\mathrm{d}\overline{T_s}}(\%\mathrm{K^{-1}})$	1.51	-0.46	1.97
$\frac{\mathrm{dCRH}}{\mathrm{d}\overline{T_s}}(\%\mathrm{K^{-1}})$	-0.62	0.27	-0.89
$\frac{\mathrm{dHCC}}{\mathrm{d}\overline{T_s}}(\%\mathrm{K^{-1}})$	-1.10	-0.19	-0.91

In order to prove that large-scale convective aggregation is the dominant process responsible for the longwave feedback difference, we use the radiative kernel approach (Soden et al., 2008) to decompose the OLR budget at each model grid cell into a contribution from: local surface temperature (T_s), atmospheric temperature (T_a), atmospheric relative humidity (RH) and cloud field.

$$\frac{\mathrm{dOLR}}{\mathrm{d}\overline{T_s}} = \frac{\partial \mathrm{OLR}}{\partial T_s}\frac{\mathrm{d}T_s}{\mathrm{d}\overline{T_s}} + \frac{\partial \mathrm{OLR}}{\partial T_a}\frac{\mathrm{d}T_a}{\mathrm{d}\overline{T_s}} + \frac{\partial \mathrm{OLR}}{\partial \mathrm{RH}}\frac{\mathrm{dRH}}{\mathrm{d}\overline{T_s}} + \text{OLR cloud feedback.} \qquad (2)$$

Note that we use surface temperature, atmospheric temperature and relative humidity rather than absolute humidity since the "lapse rate feedback" and the "specific humidity" feedback approximately cancel (Held & Shell, 2012; Jeevanjee et al., 2021). The OLR cloud feedback is computed as the residual, which is a fair estimation because we are interested in the *differences* between the two simulations (i.e. the biases in the kernel offline estimate compared to the GCM calculation can be expected to approximately cancel).

Figure 3 shows the maps of the *differences* between the two simulations of the decomposition terms in Eq. (2). The figure shows that the historical SST pattern effect on OLR is dominated by the RH contribution $\frac{\partial \mathrm{OLR}}{\partial \mathrm{RH}}\frac{\mathrm{dRH}}{\mathrm{d}\overline{T_s}}$ and the cloud feedback. They both show a decrease in OLR in the western Pacific warm pool and an increase in OLR in adjacent regions, consistent with a contraction (aggregation) of the region of deep convection. The RH contribution and the cloud feedback together account for 70% of tropical mean $\frac{\mathrm{dOLR}}{\mathrm{d}\overline{T_s}}$ ($1.01\mathrm{Wm^{-2}K^{-1}}$ in $1.45\mathrm{Wm^{-2}K^{-1}}$), and they are indeed explained by large-scale convective aggregation: The post 1980 La-Nina-like SST warming pattern (Fig. 3(f)) narrows the convective area in the western Pacific warm pool, associated with enhanced free-tropospheric drying (Fig. 3(g)) and high cloud reduction (Fig. 3(h)) in adjacent regions (especially the central Pacific). Thus, the post 1980 SST warming pattern causes enhanced OLR increase relative to uniform SST warming primarily due to large-scale convective aggregation. This finding refines previous studies that attributed the enhanced OLR increase post 1980 primarily to enhanced free-tropospheric warming (Andrews & Webb, 2018; Andrews et al., 2022).

In order to evaluate the inter-model spread of the radiative effect due to large-scale convective aggregation, we turn to the CMIP6 data archive and compare the amip-piForcing simulations (1980-2010) with the abrupt 4xCO2 simulations (150 years). The 4xCO2 simulations show a much more uniform SST warming pattern than the historical amip-piForcing

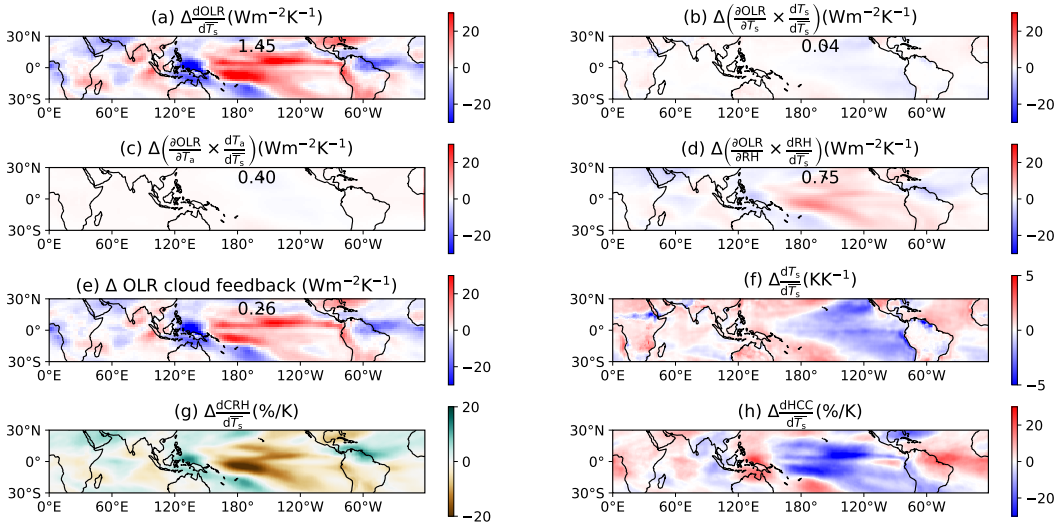

Figure 3. (a) The difference of tropical (30°S to 30°N) average OLR responses $\frac{\mathrm{dOLR}}{\mathrm{d}\overline{T_s}}$ (normalized to +1 K tropical mean surface warming) between the AM4 historical SST perturbation simulation and the uniform SST +4 K simulation (historical minus uniform +4 K), decomposed into contributions from (b) surface temperature, (c) atmospheric temperature, (d) atmosphric relative humidity and (e) could field using the radiative kernel (Equation 2), and with the tropical mean values marked in each plot. (f)(g)(h) Similar to (a) but for surface temperature (T_s), column relative humidity (CRH) and high cloud cover (HCC).

simulations, and the difference between these two experiments is the best approximation to evaluate the effect with the experiments stored in the CMIP6 archive.

For both experiments, we calculate the global mean $\frac{\mathrm{dSW_{up}}}{\mathrm{d}\overline{T_s}}$, $\frac{\mathrm{dOLR}}{\mathrm{d}\overline{T_s}}$ and $\frac{\mathrm{dOLR_{cs}}}{\mathrm{d}\overline{T_s}}$ (clear-sky OLR), using the data provided by Andrews et al. (2022). The calculations (Supplement, Table S1) show that almost all models agree that the historical La-Nina-like SST warming pattern increases $\mathrm{SW_{up}}$ *and* OLR compared to the 4x$\mathrm{CO_2}$ experiment. On average (over all models), the enhanced $\mathrm{SW_{up}}$ increase contributes to 65% ($0.83\mathrm{Wm^{-2}K^{-1}}$) of the TOA net radiation trend difference, and the enhanced OLR contributes to 35% ($0.45\mathrm{Wm^{-2}K^{-1}}$). Thus, in the multi-model mean, the two effects are of comparable magnitude.

Further, the inter-model spread of the post 1980 enhanced clear-sky OLR increase is small (ranging from $0.4\mathrm{Wm^{-2}K^{-1}}$ to $0.5\mathrm{Wm^{-2}K^{-1}}$ for most models), indicating that the large-scale aggregation and associated atmospheric drying are robust among models. Conversely, the cloud longwave radiative effect trend differences are large, and the intermodel range of the relative magnitude of the (all sky) longwave versus shortwave effect is large. For example, the calculation using the MIROC6 model attributes almost 100% of the total effect to the longwave convection aggregation effect, while the calculation using the MRI-ESM2-0 model attributes almost nothing to the longwave convection aggregation effect. Due to the physically plausible coupling between the shortwave and longwave radiative effect, one may expect a correlation between the two across models. However, this is not so ($r^2 \approx 0.1$), pointing to a need to further investigate why different models show such a large spread in the relative contribution from shortwave and longwave radiation.

4 Conclusions and discussions

The spatial pattern of tropical SST affects TOA radiation and climate sensitivity. The analysis presented here focuses on longwave radiation, complementing previous studies that focused on the shortwave cloud radiative effect (Gregory & Andrews, 2016; Zhou et al., 2017; Dong et al., 2019; Fueglistaler, 2019; Fueglistaler & Silvers, 2021; Ceppi & Fueglistaler, 2021; Williams et al., 2023). Our analysis shows that the tropical SST gradient affects OLR by modulating the strength of large-scale convective aggregation (Fig. 1 and Fig. 2): A larger SST gradient narrows the convective area, associated with the expansion of dry and clear-sky regions, both leading to an increase in OLR.

Further, we show that the large-scale convective aggregation post 1980 contributes to the enhanced OLR increase (Fig. 3) compared with a uniform SST warming case. The La-Nina-like SST warming pattern post 1980 narrows the convective area in the western Pacific warm pool compared to uniform warming, leading to free-tropospheric drying and high cloud reduction in adjacent regions (especially the central Pacific). This large-scale aggregation mechanism refines previous studies that attributed the enhanced OLR increase post 1980 primarily to enhanced free-tropospheric warming (Andrews & Webb, 2018; Andrews et al., 2022).

The enhanced OLR increase post 1980 (compared with a uniform SST warming case) is comparable to the enhanced reflected shortwave radiation in the targeted AM4 simulations (Table 1). Analysis of CMIP6 experiments shows that on average, the models have a comparable magnitude of the longwave and shortwave effect, but the inter-model spread of the partitioning is large. The notion of a warming-pattern induced anomalously negative radiative feedback since the late 1970s to the early 2000s is consistent with previous results (Zhou et al., 2016; Fueglistaler & Silvers, 2021; Armour et al., 2024). However, the large inter-model spread of net, and partitioning between long- and shortwave effect, reported here indicates a substantially larger uncertainty between models than indicated by the results of Schiro et al. (2022) who analysed the role of large-scale convective aggregation for inter-model differences in climate sensitivity. A likely explanation for the differing conclusions is that the coupled atmosphere-ocean GCMs global warming simulations analysed by Schiro et al. (2022) show only a small magnitude of the SST pattern change relative to the mean warming (Fueglistaler & Silvers, 2021). Our results reinforce the importance of large-scale convective aggregation on the radiative feedback and climate sensitivity, and highlight the need to improve understanding of the differences therein between atmospheric GCMs.

5 Open Research

The data derived from CMIP6 data can be found at `https://doi.org/10.5281/zenodo.6799004` (Andrews et al., 2022). The radiative kernel analysis follows methods provided by Chenggong Wang at `https://github.com/ChenggongWang/Radiative_Response_with_Radiative_Kernel`.

Acknowledgments

Heng Quan thanks Jing Feng, Gabriel Vecchi and Paulo Ceppi for helpful discussions. We thank Marat F. Khairoutdinov for creating and maintaining SAM.

References

Andrews, T., Bodas-Salcedo, A., Gregory, J. M., Dong, Y., Armour, K. C., Paynter, D., ... others (2022). On the effect of historical SST patterns on radiative feedback. *Journal of Geophysical Research: Atmospheres*, *127*(18), e2022JD036675.

Andrews, T., & Webb, M. J. (2018). The dependence of global cloud and lapse rate feedbacks on the spatial structure of tropical Pacific warming. *Journal of Climate*, *31*(2), 641–654.

Arakawa, A., & Schubert, W. H. (1974). Interaction of a cumulus cloud ensemble with the large-scale environment, part I. *Journal of the atmospheric sciences*, *31*(3), 674–701.

Armour, K. C., Proistosescu, C., Dong, Y., Hahn, L. C., Blanchard-Wrigglesworth, E., Pauling, A. G., ... others (2024). Sea-surface temperature pattern effects have slowed global warming and biased warming-based constraints on climate sensitivity. *Proceedings of the National Academy of Sciences*, *121*(12), e2312093121.

Becker, T., & Wing, A. A. (2020). Understanding the extreme spread in climate sensitivity within the radiative-convective equilibrium model intercomparison project. *Journal of Advances in Modeling Earth Systems*, *12*(10), e2020MS002165.

Bony, S., Semie, A., Kramer, R., Soden, B., Tompkins, A., & Emanuel, K. (2020). Observed modulation of the tropical radiation budget by deep convective organization and lower-tropospheric stability. *AGU advances*, *1*(3), e2019AV000155.

Ceppi, P., & Fueglistaler, S. (2021). The El Niño–Southern Oscillation Pattern Effect. *Geophysical Research Letters*, *48*(21), e2021GL095261.

Charney, J. G. (1963). A note on large-scale motions in the tropics. *Journal of the Atmospheric Sciences*, *20*(6), 607–609.

Chou, C., & Neelin, J. D. (2004). Mechanisms of global warming impacts on regional tropical precipitation. *Journal of climate*, *17*(13), 2688–2701.

Dong, Y., Proistosescu, C., Armour, K. C., & Battisti, D. S. (2019). Attributing historical and future evolution of radiative feedbacks to regional warming patterns using a Green's function approach: The preeminence of the western Pacific. *Journal of Climate*, *32*(17), 5471–5491.

Emanuel, K. A., David Neelin, J., & Bretherton, C. S. (1994). On large-scale circulations in convecting atmospheres. *Quarterly Journal of the Royal Meteorological Society*, *120*(519), 1111–1143.

Feng, J., Paynter, D., Wang, C., & Menzel, R. (2023). How atmospheric humidity drives the outgoing longwave radiation–surface temperature relationship and inter-model spread. *Environmental Research Letters*, *18*(10), 104033.

Fueglistaler, S. (2019). Observational evidence for two modes of coupling between sea surface temperatures, tropospheric temperature profile, and shortwave cloud radiative effect in the tropics. *Geophysical Research Letters*, *46*(16), 9890–9898.

Fueglistaler, S., & Silvers, L. (2021). The peculiar trajectory of global warming. *Journal of Geophysical Research: Atmospheres*, *126*(4), e2020JD033629.

Gregory, J. M., & Andrews, T. (2016). Variation in climate sensitivity and feedback parameters during the historical period. *Geophysical Research Letters*, *43*(8), 3911–3920.

Held, I. M., & Shell, K. M. (2012). Using relative humidity as a state variable in climate feedback analysis. *Journal of Climate*, *25*(8), 2578–2582.

Jeevanjee, N., Koll, D. D., & Lutsko, N. (2021). "simpson's Law" and the spectral cancellation of climate feedbacks. *Geophysical Research Letters*, *48*(14), e2021GL093699.

Khairoutdinov, M. F., & Randall, D. A. (2003). Cloud resolving modeling of the ARM summer 1997 IOP: Model formulation, results, uncertainties, and sensitivities. *Journal of the Atmospheric Sciences*, *60*(4), 607–625.

Klein, S. A., & Hartmann, D. L. (1993). The seasonal cycle of low stratiform clouds. *Journal of Climate*, *6*(8), 1587–1606.

Kuang, Z. (2012). Weakly forced mock Walker cells. *Journal of the Atmospheric Sci-*

ences, *69*(9), 2759–2786.

Lindzen, R. S., & Nigam, S. (1987). On the role of sea surface temperature gradients in forcing low-level winds and convergence in the tropics. *Journal of Atmospheric Sciences*, *44*(17), 2418–2436.

Lutsko, N. J. (2018). The response of an idealized atmosphere to localized tropical heating: Superrotation and the breakdown of linear theory. *Journal of the Atmospheric Sciences*, *75*(1), 3–20.

McKim, B. A., Jeevanjee, N., & Vallis, G. K. (2021). Joint dependence of longwave feedback on surface temperature and relative humidity. *Geophysical Research Letters*, *48*(18), e2021GL094074.

Muller, C. J., & Held, I. M. (2012). Detailed investigation of the self-aggregation of convection in cloud-resolving simulations. *Journal of the Atmospheric Sciences*, *69*(8), 2551–2565.

Neelin, J., Chou, C., & Su, H. (2003). Tropical drought regions in global warming and El Niño teleconnections. *Geophysical Research Letters*, *30*(24).

Quan, H., Zhang, B., Wang, C., & Fueglistaler, S. (2024). Non-linear radiative response to patterned global warming due to convection aggregation and non-linear tropical dynamics. *Journal of Climate*.

Rayner, N., Parker, D. E., Horton, E., Folland, C. K., Alexander, L. V., Rowell, D., ... Kaplan, A. (2003). Global analyses of sea surface temperature, sea ice, and night marine air temperature since the late nineteenth century. *Journal of Geophysical Research: Atmospheres*, *108*(D14).

Schiro, K. A., Su, H., Ahmed, F., Dai, N., Singer, C. E., Gentine, P., ... David Neelin, J. (2022). Model spread in tropical low cloud feedback tied to overturning circulation response to warming. *Nature Communications*, *13*(1), 7119.

Sobel, A. H., Nilsson, J., & Polvani, L. M. (2001). The weak temperature gradient approximation and balanced tropical moisture waves. *Journal of the atmospheric sciences*, *58*(23), 3650–3665.

Soden, B. J., Held, I. M., Colman, R., Shell, K. M., Kiehl, J. T., & Shields, C. A. (2008). Quantifying climate feedbacks using radiative kernels. *Journal of Climate*, *21*(14), 3504–3520.

Stevens, B., Sherwood, S. C., Bony, S., & Webb, M. J. (2016). Prospects for narrowing bounds on Earth's equilibrium climate sensitivity. *Earth's Future*, *4*(11), 512–522.

Williams, A. I., Jeevanjee, N., & Bloch-Johnson, J. (2023). Circus Tents, Convective Thresholds, and the Non-Linear Climate Response to Tropical SSTs. *Geophysical Research Letters*, *50*(6), e2022GL101499.

Wing, A. A., Emanuel, K., Holloway, C. E., & Muller, C. (2018). Convective self-aggregation in numerical simulations: A review. *Shallow clouds, water vapor, circulation, and climate sensitivity*, 1–25.

Wofsy, J., & Kuang, Z. (2012). Cloud-resolving model simulations and a simple model of an idealized Walker cell. *Journal of climate*, *25*(23), 8090–8107.

Wood, R., & Bretherton, C. S. (2006). On the relationship between stratiform low cloud cover and lower-tropospheric stability. *Journal of climate*, *19*(24), 6425–6432.

Zhang, B., Soden, B. J., Vecchi, G. A., & Yang, W. (2021). Investigating the causes and impacts of convective aggregation in a high resolution atmospheric GCM. *Journal of Advances in Modeling Earth Systems*, *13*(11), e2021MS002675.

Zhang, Y., & Fueglistaler, S. (2019). Mechanism for increasing tropical rainfall unevenness with global warming. *Geophysical Research Letters*, *46*(24), 14836–14843.

Zhang, Y., & Fueglistaler, S. (2020). How tropical convection couples high moist static energy over land and ocean. *Geophysical Research Letters*, *47*(2), e2019GL086387.

Zhang, Y., Jeevanjee, N., & Fueglistaler, S. (2020). Linearity of outgoing longwave radiation: From an atmospheric column to global climate models. *Geophysical Research Letters*, *47*(17), e2020GL089235.

Zhao, M., Golaz, J.-C., Held, I., Guo, H., Balaji, V., Benson, R., ... others (2018a). The GFDL global atmosphere and land model AM4.0/LM4.0: 1. Simulation characteristics with prescribed SSTs. *Journal of Advances in Modeling Earth Systems*, *10*(3), 691–734.

Zhao, M., Golaz, J.-C., Held, I., Guo, H., Balaji, V., Benson, R., ... others (2018b). The GFDL global atmosphere and land model AM4.0/LM4.0: 2. Model description, sensitivity studies, and tuning strategies. *Journal of Advances in Modeling Earth Systems*, *10*(3), 735–769.

Zhou, C., Zelinka, M. D., & Klein, S. A. (2016). Impact of decadal cloud variations on the earth's energy budget. *Nature Geoscience*, *9*(12), 871–874.

Zhou, C., Zelinka, M. D., & Klein, S. A. (2017). Analyzing the dependence of global cloud feedback on the spatial pattern of sea surface temperature change with a Green's function approach. *Journal of Advances in Modeling Earth Systems*, *9*(5), 2174–2189.